Science of the Total Environment 757 (2021) 143785

Contents lists available at ScienceDirect

Science of the Total Environment

journal homepage: www.elsevier.com/locate/scitotenv

Topographic Wetness Index calculation guidelines based on measured soil moisture and plant species composition

Martin Kopecký [a,b,*], Martin Macek [a], Jan Wild [a,c]

[a] Institute of Botany of the Czech Academy of Sciences, Zámek 1, CZ-252 43 Průhonice, Czech Republic
[b] Faculty of Forestry and Wood Sciences, Czech University of Life Sciences Prague, Kamýcká 129, CZ-165 21, Prague 6, Suchdol, Czech Republic
[c] Faculty of Environmental Sciences, Czech University of Life Sciences Prague, Kamýcká 129, CZ-165 21, Prague 6, Suchdol, Czech Republic

HIGHLIGHTS

- Topographic Wetness Index (TWI) quantifies terrain driven variation in soil moisture.
- TWI can be calculated with different flow-routing, slope and flow width algorithms.
- We compared these algorithms against measured soil moisture and plant composition.
- TWI algorithm determines TWI ability to predict soil moisture and plant assemblages.
- Best TWI uses Freeman flow algorithm, flow width equal cell size and local slope.

GRAPHICAL ABSTRACT

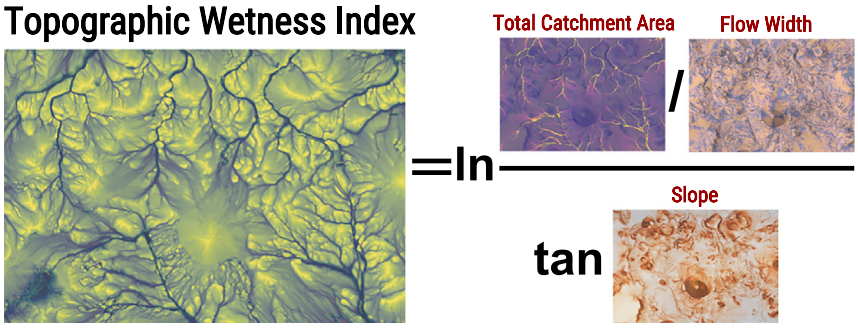

ARTICLE INFO

Article history:
Received 24 August 2020
Received in revised form 4 November 2020
Accepted 4 November 2020
Available online 14 November 2020

Editor: Manuel Esteban Lucas-Borja

Keywords:
Compound topographic index
FD8 flow routing algorithm
Forest bryophytes
SAGA wetness index
TMS microclimate logger
Volumetric water content

ABSTRACT

Soil moisture controls environmental processes and species distributions, but it is difficult to measure and interpolate across space. Topographic Wetness Index (TWI) derived from digital elevation model is therefore often used as a proxy for soil moisture. However, different algorithms can be used to calculate TWI and this potentially affects TWI relationship with soil moisture and species assemblages.

To disentangle insufficiently-known effects of different algorithms on TWI relation with soil moisture and plant species composition, we measured the root-zone soil moisture throughout a growing season and recorded vascular plants and bryophytes in 45 temperate forest plots. For each plot, we calculated 26 TWI variants from a LiDAR-based digital terrain model and related these TWI variants to the measured soil moisture and moisture-controlled species assemblages of vascular plants and bryophytes.

A flow accumulation algorithm determined the ability of the TWI to predict soil moisture, while the flow width and slope algorithms had only a small effects. The TWI calculated with the most often used single-flow D8 algorithm explained less than half of the variation in soil moisture and species composition explained by the TWI calculated with the multiple-flow FD8 algorithm. Flow dispersion used in the FD8 algorithm strongly affected the TWI performance, and a flow dispersion close to 1.0 resulted in the TWI best related to the soil moisture and species assemblages. Using downslope gradient instead of the local slope gradient can strongly decrease TWI performance.

Abbreviations: DEM, Digital Elevation Model; LiDAR, Light Detection And Ranging; RMSE, Root Mean Square Error; TWI, Topographic Wetness Index.

* Corresponding author at: Institute of Botany of the Czech Academy of Sciences, Zámek 1, CZ-252 43, Průhonice, Czech Republic.
E-mail address: ma.kopecky@gmail.com (M. Kopecký).

https://doi.org/10.1016/j.scitotenv.2020.143785

Our results clearly showed that the method used to calculate TWI affects study conclusion. However, TWI calculation is often not specified and thus impossible to reproduce and compare among studies. We therefore provide guidelines for TWI calculation and recommend the FD8 flow algorithm with a flow dispersion close to 1.0, flow width equal to the raster cell size and local slope gradient for TWI calculation.

1. Introduction

Soil moisture affects key environmental processes and controls plant growth, distribution and community assembly (Fan et al., 2019; Kemppinen et al., 2019; le Roux et al., 2013). In particular, long-term soil moisture measurements are ecologically crucial, because plants reflect soil moisture integrated over time (Breshears et al., 2009). However, long-term soil moisture is difficult to measure (Babaeian et al., 2019; Robinson et al., 2008) and interpolate across space (Kemppinen et al., 2018; Lookingbill and Urban, 2004; Martin et al., 2017). To overcome these limitations, researchers use soil moisture proxies derived from Digital Elevation Models (DEM). Undoubtedly, the most popular is a Topographic Wetness Index (Beven and Kirkby, 1979).

Topographic Wetness Index (TWI) integrates the water supply from upslope catchment area and downslope water drainage for each cell in a DEM (Fig. 1). In the TWI, the slope gradient approximates downslope water drainage, and the specific catchment area, calculated as the total catchment area divided by the flow width, approximates the water supply from upslope area (Beven and Kirkby, 1979). The TWI therefore has three key components: total catchment area, flow width and slope gradient (Fig. 1). The total catchment area represents the cumulative upslope area that drains through the cell calculated with the flow routing algorithm, the flow width is the length of a contour orthogonal to the flow from the cell, and the slope gradient is either the slope of the focal cell or the slope between the focal cell and a cell further downslope (Gruber and Peckham, 2009).

While simple and intuitive, TWI performs well in a wide range of applications (Moore et al., 1991; Wilson, 2018), and thanks to the increasing availability of high-resolution DEMs, it can be calculated on ecologically relevant scales for even the most remote regions (Stichbury et al., 2011; Wietrzyk-Pełka et al., 2020). Many different algorithms can be however used to calculate all three TWI components – total catchment area, flow width and slope gradient (Gruber and Peckham, 2009; Wilson, 2018). While the differences among these

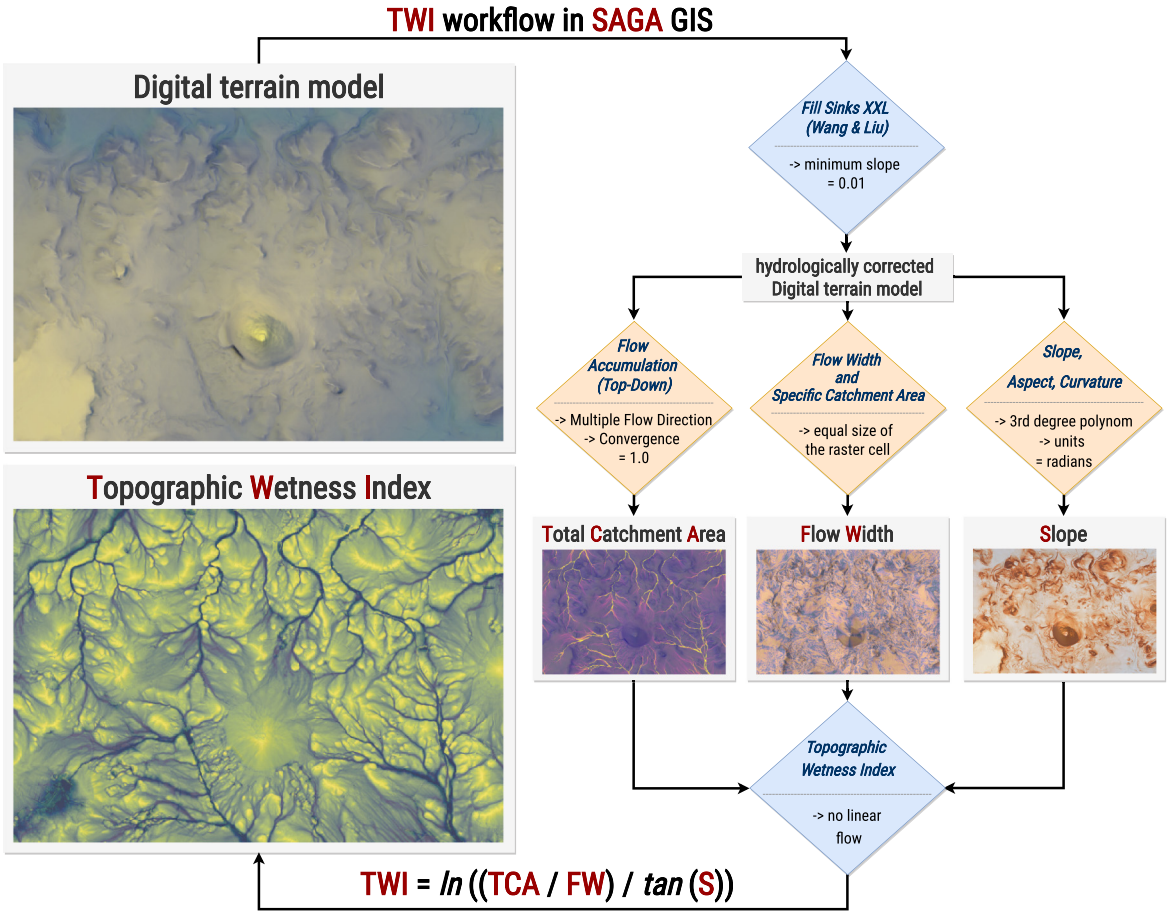

Fig. 1. Topographic Wetness Index (TWI) expresses the terrain-driven balance of the catchment water supply and local drainage. When calculating the TWI from the digital terrain model, all terrain sinks and flat pixels should be removed first. Then, total catchment area, flow width and slope for each pixel must be calculated. Finally, these three components are integrated into the TWI according to the equation shown in the bottom. The schema shows the TWI workflow in SAGA GIS, where the diamonds represent the geoprocessing tools, the blue font indicates the names of the tools and the text specifies the settings producing the TWI best correlated with soil moisture according our results. The orange diamonds highlight the three TWI components evaluated in this study.

algorithms may appear to be rather technical details, they are actually not because they result in different slopes (Jones, 1998; Tang et al., 2013; Warren et al., 2004), catchment areas (Erskine et al., 2006; Wilson et al., 2007; Zhou and Liu, 2002) and TWI patterns (Gruber and Peckham, 2009; Pan et al., 2004; Wolock and McCabe, 1995).

Despite the wide range of algorithms currently used, only a few studies have explored how the algorithm choice affects the relationship between TWI and soil moisture (Buchanan et al., 2014; Raduła et al., 2018; Sørensen et al., 2006). Using a snapshot measurements of soil water content, these studies found large differences among methods for calculating the TWI. However, temporal fluctuations in soil water content modify the relationship between soil moisture and the TWI (Beaudette et al., 2013; Oroza et al., 2018; Western et al., 1999; Yeakley et al., 1998). Long-term soil moisture measurements are therefore urgently needed to evaluate the performance of different methods for calculating TWI.

While the TWI is increasingly used in ecology (Muscarella et al., 2020; Schmitt et al., 2020; Schwantes et al., 2018) and in environmental sciences (Greiser et al., 2018; Metzen et al., 2019; Piedallu et al., 2019), its calculation is often not specified, and the rationale for choosing a particular TWI method is rarely discussed. To date, only one study has compared different TWI calculation methods against multidimensional species data and found that the TWI calculated with the FD8 flow algorithm explained plant species composition substantially better than other flow algorithms (Kopecký and Čížková, 2010). However, other plant-relevant variables, such as air temperature and nutrient availability, also correlate with the TWI (Macek et al., 2019; Seibert et al., 2007; Vanwalleghem and Meentemeyer, 2009; Zinko et al., 2006). The higher compositional variation explained by the FD8 flow algorithm, therefore, does not necessarily mean a more direct link with moisture-driven patterns in plant assemblages. As a result, the potential links among different TWI calculation methods, soil moisture and plant species composition are still largely unknown.

To fill this knowledge gap, which hampers more informed use of the TWI, we disentangled the effects of 12 flow, 10 slope and 4 flow width algorithms on the ability of the TWI to predict soil moisture measured in 45 forest plots continually throughout a growing season. Using in-situ measured soil moisture and plant species composition, we further explored how TWIs calculated with different algorithms explain the moisture-controlled composition of two groups of primary producers with contrasting ecological requirements: vascular plants and bryophytes. Based on our results, we provided simple guidelines for robust TWI calculation and reporting.

2. Materials and methods

2.1. Study area

We studied the relationships among the TWI, soil moisture and plant assemblages in temperate broadleaved forests in the northwestern part of the Czech Republic (Fig. 2). The dynamic terrain of this area includes both steep slopes of volcanic hills rising above the undulating plateau formed by tertiary sediments and deeply incised valleys draining the plateau to the Elbe River canyon. Elevations range from 122 m a.s.l. near the Elbe River to 837 m a.s.l. at the top of the Milešovka hill. The climate is temperate, with a mean annual temperature ranging from 5 to 9 °C, a mean annual precipitation of 450–600 mm and prevailing westerly winds. The typical forest soils are Cambisols and Luvisols, mostly with a silt-loam texture.

2.2. Field sampling

We established a network of permanent plots across topographically complex landscape (Fig. 2) using random sampling within strata defined by elevation, potential solar radiation and topographic wetness (Macek et al., 2019). In 45 plots, we measured the soil water content every 15 min throughout the growing season, starting on 1st May and ending on 30th September 2017. We measured the water content in the upper 15 cm of mineral soil, as this represents the root zone most relevant for temperate forest plants (Goebes et al., 2019).

To measure the soil water content, we used TMS loggers, version 4, with accurate moisture sensors based on time domain transmission (Wild et al., 2019). To transform the TMS measurements to volumetric soil water content, we used a calibration curve developed from laboratory measurements (Appendix A).

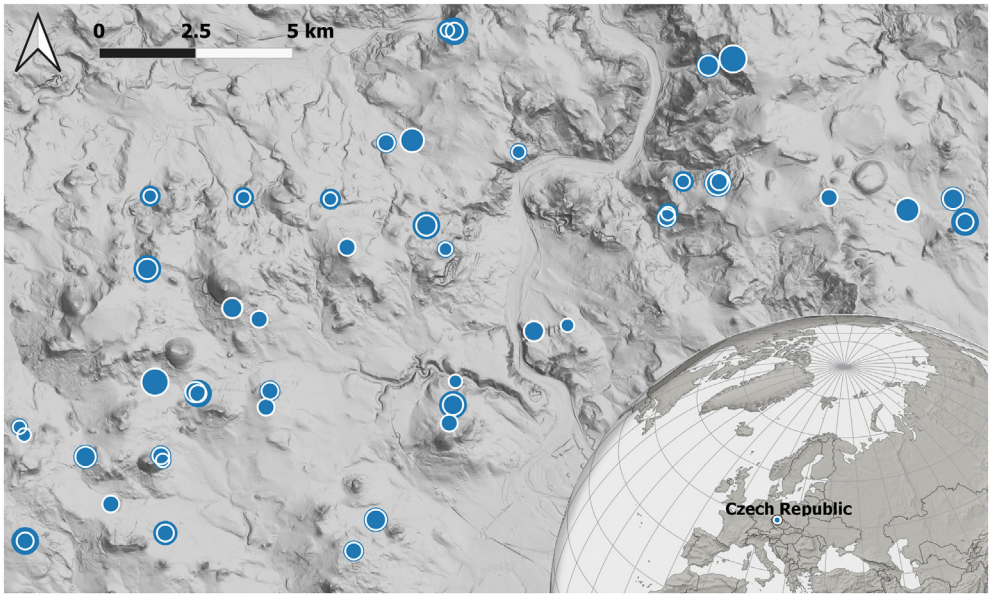

Fig. 2. Terrain of the study area in the northwestern part of the Czech Republic. The blue dots show the 45 study sites established in temperate broadleaved forests. The size of each blue dot is proportional to the growing-season mean volumetric water content in the root zone, and the size of the white circles is proportional to Topographic Wetness Index calculated with the FD8q flow algorithm. Background represents hillshade of the digital terrain model used to calculate TWI.

We used a differential GPS to measure the geographic coordinates of each TMS logger under leaf-off conditions. To further increase coordinate precision, we post-processed the field measurements with simultaneous measurements taken at the nearest geodetic station of the Czech Office for Surveying, Mapping and Cadastre.

In the 100 m^2 area surrounding each TMS logger, we recorded the species composition of two ecologically contrasting groups of primary producers: vascular plants and bryophytes. The percentage cover of each species was visually estimated and taxonomically difficult specimens were collected and subsequently identified in the laboratory.

One plot did not contain any bryophyte species; therefore, we analysed the species composition of all 45 plots with vascular plants and 44 plots with bryophytes. In these plots, we recorded 186 species of vascular plants (median per plot = 24, min = 4, max = 54) and 44 species of bryophytes (median = 10, min = 6, max = 18).

2.3. TWI calculation

To calculate 26 TWI variants (Table 1), we followed the TWI workflow (Fig. 1) in open-source SAGA GIS ver. 7.4 (Conrad et al., 2015). As a digital elevation model, we used a national LiDAR-based terrain model with a 5 m horizontal and 1 cm vertical resolution (Fig. 2). Because flow algorithms artificially stop when they encounter terrain depressions without outlets, we filled the terrain sinks with the *Fill Sinks XXL* function, which is suitable for processing LiDAR DEMs (Wang and Liu, 2006). To prevent division by zero during TWI calculation, we set the minimal slope in the filled DEM to 0.01°. This pre-processing, however, did not affect the slope values extracted for our plots because they all lie outside the modified parts of the DEM (Fig. 3).

Previous results suggested that the flow algorithm used to calculate the total catchment area can strongly affect the relationship between the TWI and soil moisture (Sørensen et al., 2006; Buchanan et al., 2014). Therefore, we first compared the ability of TWIs calculated with different flow algorithms to predict soil moisture. We used all 12 flow algorithms available in SAGA to calculate 12 variants of the total catchment area (Table 1). Then, we converted these total catchment areas to specific catchment areas using the flow width calculated with the SAGA default method based on cell aspect (Gruber and Peckham, 2009). From pre-processed DEM, we calculated the slope in radians using the SAGA default method (Zevenbergen and Thorne, 1987). Finally, we combined this slope with all 12 variants of the specific catchment areas into 12 TWI grids differing only in the flow algorithm used to calculate the total catchment area.

Different slope algorithms produce different slope estimates from the same DEM (Jones, 1998; Tang et al., 2013; Warren et al., 2004), however, it is unknown whether this affects the ability of the TWI to predict soil moisture. Therefore, we combined the specific catchment area calculated with the best flow algorithm with six different slope algorithms (Table 1) and explored the ability of the resulting TWIs to predict the measured soil moisture.

Using the local slope during the calculation of the TWI assumes that the local water table is parallel to the soil surface (Gruber and Peckham, 2009). Because this assumption is often unrealistic (Lanni et al., 2011), the local slope gradient can be replaced with a downslope gradient expressing the slope to the nearest downslope cell that is *d* metres below

Table 1
Overview of the 12 flow accumulation, 10 slope and 4 flow width algorithms compared in this study. All algorithms are available in the SAGA GIS.

Algorithm	Abbreviation	Description	Reference
Flow accumulation			
Deterministic single-flow	D8	Flow routed to the steepest downslope cell	O'Callaghan and Mark (1984)
Stochastic single-flow	Rho8	Flow to one downslope cell randomly selected with probability proportional to the slope between the cells	Fairfield and Leymarie (1991)
Aspect driven kinematic routing	KRA	Flow routed like a ball released from the centre of the cell and rolling on a plane fitted to the cell corners	Lea (1992)
DEM networks	DEMON	Flow is routed over a plane fitted for each focal cell according elevations of the surrounding cells	Costa-Cabral and Burges (1994)
Braunschweiger reliefmodell	BR	Flow routed to the downslope cell with the most similar aspect and its two neighbouring cells	Bauer et al. (1985)
Determinictic infinity	Dinf	Flow into one or two neighbours depending on flow direction determined by the steepest descent	Tarboton (1997)
Multiple-flow Dinf	MDinf	Like Dinf, but allowing flow to all downslope cells, flow dispersion set to 1.0	Seibert and McGlynn (2007)
Multiple-flow Freeman	FD8f	Flow to all downslope cells, the flow amount given by the slope between the target and the source cell, flow dispersion = 1.1	Freeman (1991)
Multiple-flow Quinn	FD8q	FD8f with flow dispersion = 1.0, different from the original Quinn et al. method, which used different flow width into cardinal and diagonal cells	Quinn et al. (1991)
Multiple-flow Holmgren	FD8h	FD8f with flow dispersion = 6.0	Holmgren (1994)
Multiple-flow based on downslope gradient	FD8-md	FD8f with cell-specific flow dispersion based on maximum downslope gradient	Qin et al. (2007)
Iteratively modified FD8f	SAGA	FD8f flow adjusted according the maximum flow accumulation in the surrounding cells with small slopes, algorithm specific to SAGA GIS	Böhner and Selige (2006)
Slope gradient			
Maximum slope	maxS	Slope to the lowest neighbouring cell	Travis et al. (1975)
Maximum triangle slope	maxTS	Maximum slope in a triangular facet	Tarboton (1997)
Horn	Horn	Least squares fitted plane	Horn (1981)
Heerdegen and Beran	HaB	2nd degree polynomial with 6 parameters	Heerdegen and Beran (1982)
Zevenbergen and Thorne	ZaT	2nd degree polynomial with 9 parameters	Zevenbergen and Thorne (1987)
Haralick	Haralick	3nd degree polynomial with 10 parameters	Haralick (1983)
Downslope gradient 5 m	DG_5	Calculated over 5 m vertical distance	Hjerdt et al. (2004)
Downslope gradient 10 m	DG_10	Calculated over 10 m vertical distance	Hjerdt et al. (2004)
Downslope gradient 20 m	DG_20	Calculated over 20 m vertical distance	Hjerdt et al. (2004)
Downslope gradient 30 m	DG_30	Calculated over 30 m vertical distance	Hjerdt et al. (2004)
Flow width			
D8-based	D8	Different flow width for cardinal and diagonal cells	O'Callaghan and Mark (1984)
Quinn	Quinn	Cumulative flow width to all downslope cells	Quinn et al. (1991)
Aspect-based	Aspect	Continual flow width based on cell aspect	Gruber and Peckham (2009)
Pseudo-specific	Pseudo	Flow width equal to the size of the grid cell	Chirico et al. (2005)

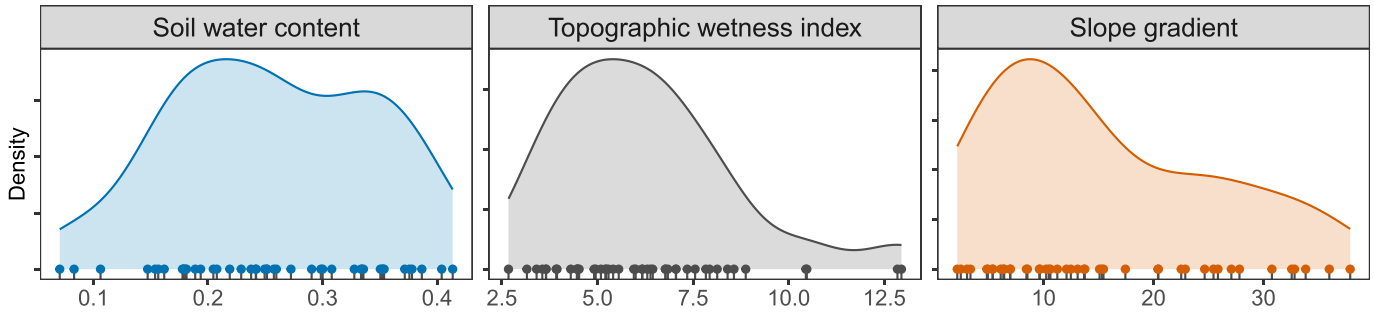

Fig. 3. Overview of the volumetric soil water content, Topographic Wetness Index (TWI) and slope gradient in the 45 sampled plots. Each panel shows both the overall distribution of the values calculated as the kernel density of the observations along the x axis (shaded area) and exact values for each sampled plot (bottom rug). The TWI was calculated with the FD8q algorithm and slope gradient in degrees with the Zevenbergen-Thorne method.

the focal cell (Hjerdt et al., 2004). The *d* value thus controls the deviation of the local water table from the local slope and must be subjectively specified during calculation. Despite theoretical advantages, it is not clear whether the replacement of local slope with downslope gradient improves the ability of the TWI to predict soil moisture (Buchanan et al., 2014). To explore this, we also calculated four downslope gradient variants differing in the *d* value (Table 1) and compared the performance of the resulting TWIs with that of the TWIs based on the local slope gradients.

Finally, it is unknown whether the method used to calculate the local flow width affects ability of the TWI to predict soil moisture. Therefore, we explored whether four different methods of the flow width calculation (Table 1) affect the ability of the TWI to predict soil moisture. To focus solely on the effects of flow width algorithms, we used the best performing flow algorithm to calculate the total catchment area and the default Zevenbergen-Thorne algorithm to calculate the slope.

2.4. TWI and soil moisture

To explore how the TWIs calculated with different methods explain soil moisture, we calculated the spatial variance in the mean soil water content explained by each TWI method with a linear regression model implemented with the *lm* function in R ver. 3.5.1 (R Core Team, 2020).

To get robust estimates of the explained variance, we used bootstrapping. First, we randomly assembled the 45 plots in our dataset using the *sample* function in R. Then, we calculated the variance in the measured soil moisture explained by each TWI variant in this randomly assembled dataset. We repeated this procedure 1000 times and finally calculated the mean and associated confidence intervals for each TWI variant.

To further evaluate the predictive ability of the TWI variants, we calculated the mean root mean square error (RMSE) of the soil moisture prediction with the TWI based on leave-one-out cross-validation. Specifically, we first fit the linear model based on all plots except one, then used the fitted model to predict soil moisture at the plot that was previously excluded from model fitting and finally calculated the RMSE from the predicted and observed soil moisture.

To explore whether the different TWI algorithms have consistent ability to explain and predict also the driest soil conditions during the growing season (i.e. soil drought), we calculated the explained variance and leave-one-out RMSE also for the 5th percentile of the soil moisture measurements on each TMS logger.

2.5. TWI and moisture-controlled species assemblages

We explored how different TWI variants explain the assemblages of vascular plants and bryophytes structured along the soil moisture gradient. To analyse differences in species composition rather than differences in total species cover among the sites, we first square-rooted species percentage cover data, then standardised them by the total cover of all the species present within each plot and finally calculated Bray-Curtis dissimilarity matrix from these proportional cover data.

First, we explored whether the mean soil moisture or soil drought during the growing season is more tightly linked to species composition. Separately for vascular plants and bryophytes, we calculated the proportion of the compositional variation explained by mean soil moisture and soil drought in a distance-based RDA applied to Bray-Curtis dissimilarity matrix (McArdle and Anderson, 2001). Because soil drought explained more compositional variation in both groups (mean soil moisture explained 94.8% and 88.3% of variation explained by soil drought for vascular plants and bryophytes, respectively), we used soil drought in the following analyses.

To focus on moisture-controlled species composition, we first calculated the compositional variation explained by the measured soil moisture in a distance-based RDA applied to Bray-Curtis dissimilarity matrix. Then, we calculated the proportion of this moisture-controlled variation explained by each TWI variant using the variation partitioning (Legendre and Lengendre, 2012) implemented with the *vegan* R package (Oksanen et al., 2019). Finally, to get robust estimates, we repeated this variation partitioning on 1000 bootstrapped datasets for each group of primary producers.

3. Results

TWI was able to explain slightly more variation in mean soil moisture than in soil drought and the models for mean soil moisture have had also lower cross-validated RMSE (Table 2). Nevertheless, the relative performance of TWI calculation methods was comparable between models of mean soil moisture and soil drought and the same TWI algorithms were able to explain and predict mean soil moisture and soil drought better than others (Table 2).

3.1. Flow accumulation

The flow algorithm used to calculate the total catchment area determined the ability of the TWI to explain (Fig. 4a) and predict (Table 2) the in-situ measured soil moisture. Single-flow algorithms (e.g., D8 and KRA) performed generally worse than multiple-flow algorithms (e.g., FD8 and MDinf). The best performing multiple-flow algorithms explained more than twice as much variance in the measured soil moisture than the worst single-flow algorithms, both in the original (Table 2) as well as in the bootstrapped datasets (Fig. 4a). While the linear model with the best predicting ability based on FD8q flow algorithm has a mean RMSE of 5.99% of the mean volumetric water content, the most often used algorithm (D8) has a RMSE of 6.71%, and the worst performing algorithm (Rho8) has a RMSE of 6.82% (Table 2).

The four best performing algorithms were all based on the FD8 algorithm and differ only by the flow dispersion value controlling flow

Table 2
Ability of different TWI calculation methods to explain and predict mean soil moisture in a growing season and soil drought calculated as the 5th percentile of the soil moisture measurements on each TMS logger. R^2 is the variance explained by each TWI variant in linear regression model and RMSE is mean root mean square error based on leave-one-out cross-validation. The flow algorithm has the largest effect; therefore, the same flow algorithm (FD8q) was used for the comparison of the slope and flow width algorithms. Within each category, algorithms are sorted according to decreasing explained variance.

Algorithm	Abbreviation	Mean soil moisture		Soil drought	
		R^2	RMSE	R^2	RMSE
Flow accumulation					
Multiple-flow Quinn	FD8q	0.3181	0.0598	0.3015	0.0659
Multiple-flow Freeman	FD8f	0.3163	0.0599	0.2998	0.0660
Multiple-flow based on downslope gradient	FD8-md	0.3010	0.0612	0.2867	0.0672
Multiple-flow Holmgren	FD8h	0.2424	0.0642	0.2375	0.0688
Multiple-flow Dinf	MDinf	0.2033	0.0658	0.2077	0.0703
Determinictic infinity	Dinf	0.1988	0.0652	0.1812	0.0706
Braunschweiger reliefmodell	BR	0.1851	0.0659	0.1658	0.0707
Deterministic single-flow	D8	0.1504	0.0671	0.1560	0.0707
Aspect driven kinematic routing	KRA	0.1461	0.0665	0.1448	0.0706
Stochastic single-flow	Rho8	0.1455	0.0682	0.1300	0.0735
DEM networks	DEMON	0.1429	0.0669	0.1398	0.0714
Iteratively modified FD8f	SAGA	0.1285	0.0665	0.1220	0.0724
Slope gradient					
Haralick	Haralick	0.3220	0.0598	0.3039	0.0658
Heerdegen and Beran	HaB	0.3213	0.0599	0.3036	0.0658
Horn	Horn	0.3207	0.0599	0.3032	0.0659
Zevenbergen and Thorne	ZaT	0.3181	0.0598	0.3015	0.0659
Maximum triangle slope	maxTS	0.3143	0.0588	0.3005	0.0650
Maximum slope	maxS	0.3142	0.0588	0.3004	0.0650
Downslope gradient 30 m	DG_30	0.3094	0.0609	0.3083	0.0668
Downslope gradient 20 m	DG_20	0.3089	0.0608	0.3071	0.0667
Downslope gradient 10 m	DG_10	0.2991	0.0606	0.2928	0.0666
Downslope gradient 5 m	DG_5	0.2772	0.0604	0.2672	0.0666
Flow width					
Pseudo-specific	Pseudo	0.3207	0.0596	0.3057	0.0656
Aspect-based	Aspect	0.3181	0.0598	0.3015	0.0659
Quinn	Quinn	0.3144	0.0596	0.2992	0.0660
D8-based	D8	0.3140	0.0594	0.2975	0.0653

partitioning into surrounding cells. The multiple-flow FD8 algorithms with weaker flow convergence (FD8q and FD8f) performed significantly better than the FD8h algorithms with stronger flow convergence (Table 2). Recent FD8 modification that use different flow dispersion for each cell (FD8-md) explained soil moisture significantly worse than the FD8q and FD8f algorithms, which use fixed flow dispersion (Fig. 4a).

The SAGA wetness index – a popular TWI variant that use iteratively modified catchment area, explained less variance both in the mean and minimum soil water content than any other TWI method (Table 2). The SAGA wetness index first calculates total catchment area with the FD8f flow algorithm, and then modify this catchment area iteratively according the maximum catchment area in the surrounding flat terrain. This modification however decreased SAGA wetness index performance, because SAGA wetness index explained less than half of the variance in the measured soil moisture and had lower predictive ability than the TWI based on the unmodified catchment area calculated with the FD8f flow algorithm (Table 2).

This is also supported by the better average performance of the SAGA wetness index in bootstrapped datasets (Fig. 4a). During bootstrapping, algorithm sometimes assembled only sites with original unmodified catchment area and such TWI therefore performed as well as TWI based on FD8f algorithm. On the other hand, when bootstrapping algorithm assembled mostly sites with modified catchment area, the SAGA wetness index performed poorly.

3.2. Local slope and downslope gradient

The slope algorithms affected the ability of the TWI to predict soil moisture substantially less than the flow algorithms (Table 2). While all the TWI variants calculated with six different local slope algorithms explained comparable variance, replacing the local slope with the downslope gradient affected the ability of the TWI to predict soil moisture (Fig. 4b). The TWI variants based on downslope gradients calculated over 5 m and 10 m performed significantly worse than those based on the local slope, while the variants based on downslope gradients calculated over 20 m and 30 m performed comparably to those based on the local slope (Fig. 4b).

3.3. Flow width

Different flow width algorithms had consistent but small effects on the ability of the TWI to predict the measured soil moisture (Table 2). Interestingly, the pseudo-specific catchment area (i.e., the total catchment area divided by the raster cell size) performed better than specialised algorithms that use variable flow width for each cell (Fig. 4c).

3.4. Species composition

Different TWI variants explained strikingly different amounts of variation in the moisture-controlled species composition and the ranking of the TWI variants was comparable between the vascular plants and bryophytes (Fig. 5). The best performing FD8 multiple-flow algorithms explained three times more variation in the moisture-controlled species composition than the worst algorithm (Rho8), both for vascular plants and bryophytes. The most often used algorithm (D8) explained less than half of the variation explained by the FD8 algorithms (Fig. 5).

4. Discussion

We found that differently calculated TWI explained the in-situ measured soil moisture and moisture-controlled plant species composition differently and the same TWI calculation method best predicted the soil moisture and vascular plant and bryophyte species assemblages. The method of TWI calculation thus determines the study results.

In ecology, most studies do not sufficiently specify the methods used to calculate the TWI, and many do not specify them at all (Kopecký and Čížková, 2010). However, our results clearly showed that studies based on differently calculated TWI are not comparable and – when the method used to calculate the TWI is not specified – not reproducible. We therefore argue for change in this practice and use our results to provide guidelines for TWI calculation and reporting (summarized in Fig. 1).

4.1. Flow algorithm matters most

The flow algorithm determined the ability of the TWI to predict soil moisture and plant species composition. Single-flow algorithms often result in artificial patterns in TWIs, especially on convex landforms and hillslopes (Erskine et al., 2006; Pan et al., 2004; Wilson et al., 2007), and TWIs calculated with single-flow algorithms therefore predict soil moisture worse than TWIs based on multiple-flow algorithms (Raduła et al., 2018; Sørensen et al., 2006). Single-flow algorithms also performed worse in dynamic ecosystem models (Tang et al., 2015) and are also less correlated with the plant species composition in temperate forests (Kopecký and Čížková, 2010).

Despite these findings, single-flow algorithms are the default - and often the only - algorithms implemented in many GIS programs - for example in widely used ArcGIS, and in dedicated R packages such as *topmodel* (Buytaert et al., 2008), *dynatopmodel* (Metcalfe et al., 2015) or *ecohydrotools* (Maclean, 2020). Especially the recent advances in R

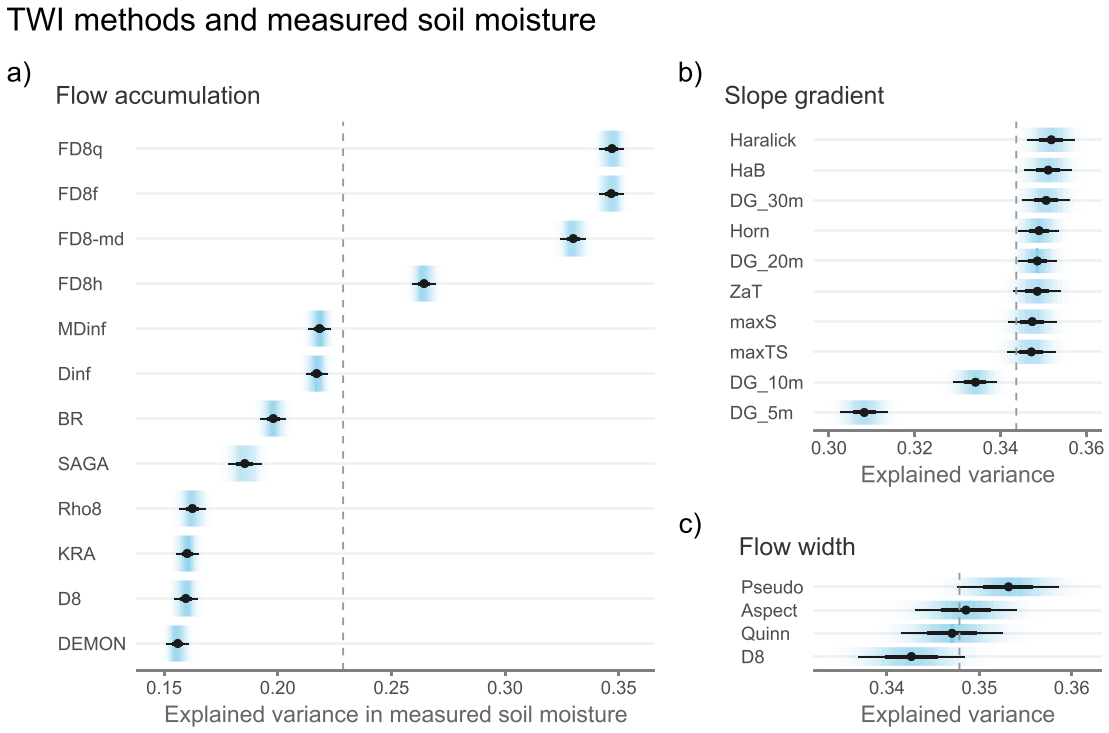

Fig. 4. Ability of different TWI calculation methods to explain mean soil moisture during the growing season. The black points represent the mean variance in soil moisture explained by each TWI variant over 1000 bootstrapped datasets. The thick lines represent the 66% confidence intervals around the means, while the thin lines and blue shading represent the 95% confidence intervals around the means. The dashed vertical lines show the overall mean across all the TWI variants. The flow algorithm has the largest effect; therefore, the same flow algorithm (FD8q) was used for the comparison of the slope and flow width algorithms.

geocomputation abilities make semi-automatic TWI calculation increasingly popular (e.g. Huntley et al., 2017; McGregor et al., 2020; Muscarella et al., 2020). However, most R packages for TWI calculation implement only single-flow routing algorithms like D8. According to our results, researchers can increase the explanatory power and ecological realism of their models by calculating TWI with the FD8 multiple-flow algorithms.

The best performing flow algorithms were all FD8 algorithms, which differed only by the dispersion coefficient used to partition the flow into the neighbouring downslope cells. We found that the flow dispersion values close to 1.0, either 1.0 in FD8q or 1.1. in FD8f, performed substantially better than the higher values recommended by Holmgren (1994). This seemingly small detail about the flow dispersion again illustrates how important it is to specify the

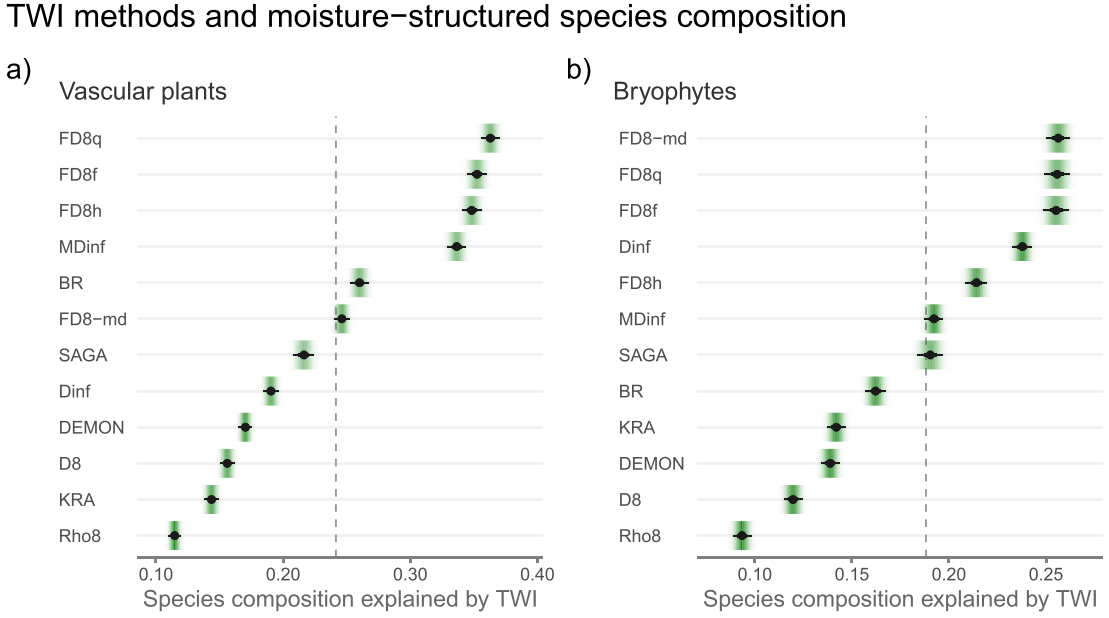

Fig. 5. Ability of different TWI calculation methods to explain moisture-controlled species composition of vascular plants and bryophytes. The black points represent the mean proportion of the explained variation in 1000 bootstrapped datasets. The thick lines represent the 66% confidence intervals around the means, and the thin lines and green shading represent the 95% confidence interval around the means. The dashed vertical lines show the overall mean across all the TWI variants.

method used for TWI calculation. For example, the popular GRASS module *r.watershed* can calculates total catchment area with the best-performing FD8 algorithms, but the default flow dispersion value is five (Mattivi et al., 2019). As we found, GRASS and QGIS users can easily calculate TWI with better predictive ability by lowering the default flow dispersion value.

The algorithm used to calculate the local slope had only a small effect on the TWI performance and the local slope performs as well as the optimally selected downslope gradient, despite the theoretical advantages of the later (Hjerdt et al., 2004; Lanni et al., 2011). The TWIs based on 20 and 30 m downslope gradients explained significantly more variance than 5 and 10 m downslope gradients, while the TWI based on shorter downslope gradients better explained soil moisture in less topographically heterogeneous regions (Buchanan et al., 2014; Hjerdt et al., 2004). The optimal distance for downslope gradient calculation is therefore site-specific and when the distance is chosen sub-optimally, the TWI calculated with downslope gradient predicts soil moisture worse than the TWI calculated with local slope (Sørensen et al., 2006). We therefore think that the local slope should be preferred during TWI calculation.

The ability of the TWI to predict soil moisture was also affected by the method used to calculate the flow width, but the effect of this parameter was small. This finding is new and important, because most GIS programs and dedicated R packages do not implement flow width algorithms. Many studies therefore calculated TWI with total, instead of specific, catchment area (Lookingbill and Urban, 2004; Schwantes et al., 2018; Vanwalleghem and Meentemeyer, 2009). Such TWI is, however, conceptually different from the TWI described by Beven and Kirkby (1979) and strongly depends on grid resolution (Sørensen and Seibert, 2007). Given the ease with which pseudo-specific catchment area can be calculated in any software, we strongly argue against the use of TWI based on the total catchment area. By dividing total catchment area by the grid cell size, researchers can benefit from the advantages of TWI based on specific catchment area and simultaneously increase the comparability of their results.

4.2. SAGA wetness index

Increasingly popular TWI calculation method specific to SAGA GIS - and therefore called the SAGA Wetness Index - explained less than half of the variance in soil moisture as the TWI calculated with the same FD8f flow algorithm. During the catchment area adjustment used in the SAGA Wetness Index, flow accumulation in the relatively flat grid cells is iteratively replaced by the maximum flow accumulation in the surrounding grid cells (Böhner and Selige, 2006). The result is a higher and more uniform catchment area in a topographically flat areas such as valley bottoms, theoretically better reflecting a high water table near the flow channels (Böhner and Selige, 2006). However, in our study area, this catchment adjustment substantially decreased the ability of the TWI to explain soil moisture. Therefore, the claim often copied from SAGA GIS documentation that the SAGA Wetness Index predicts "a more realistic, higher potential soil moisture compared to the standard TWI calculation" needs to be tested. Thus far, the evidence suggests that the SAGA Wetness index predicts soil moisture worse than the classical TWI calculated with multiple-flow FD8 algorithm.

4.3. Species assemblages

Soil drought expressed as 5th percentile of soil moisture measurements during the growing season explained more variation in vascular plant and bryophyte species composition than mean soil moisture during the growing season. This points to the soil drought as an important factor shaping forest plant communities, so far showed mostly for tree species assemblages (Ackerly et al., 2020; McLaughlin et al., 2020; Piedallu et al., 2013). While TWI was able to explain and predict slightly less variation in soil drought than in mean soil moisture, relative performance of TWI calculation methods was comparable between models of mean soil moisture and soil drought. TWI calculation method has therefore important effects also when modelling soil drought and its impact on vegetation.

For the first time, we also showed the importance of TWI calculation methods for the prediction of bryophyte assemblages. This is important, as bryophytes are highly sensitive to the microscale variations in soil moisture, and TWI is increasingly used as a proxy for this variation (Moeslund et al., 2019; Zellweger et al., 2015). As is often the case, both cited studies used a TWI calculated with the single-flow D8 algorithm. However, the D8 algorithm was the second worst in our comparison and the TWI based on the FD8q multiple-flow algorithm explained three times more variation in the moisture-controlled bryophyte species composition. Therefore, the relative importance of topographically controlled soil moisture would be even higher, if these studies calculated the TWI with the FD8 instead of the D8 algorithm.

We found that the ranking of the TWI algorithms according their ability to explain species composition is comparable between the bryophytes and vascular plants despite their different ecology. As the overall ranking of the TWI algorithms agree well with results from other temperate regions (Kopecký and Čížková, 2010; Raduła et al., 2018), the performance of different TWI algorithms seems consistent among different regions and taxonomic groups. However, only a few studies have compared different TWI algorithms against species compositional data or measured soil moisture, and further testing in different habitats and under different macroclimatic conditions is therefore needed.

5. Conclusion

Flow algorithm determine TWI ability to predict soil moisture and plant species composition. The amount of explained variation doubled when the TWI was calculated with the Freeman multiple-flow FD8 algorithm instead of the most widely used D8 algorithm. Given such a different performance, it is surprising that only a minority of studies have reported the methods used for TWI calculation. While it is hard to imagine that reviewers and editors will allow authors to write that they used "mixed effect model" or "multivariate ordination" without any further specification, exactly this happens with TWI. However, without sufficient specification of the methods used to calculate the TWI, studies are not reproducible and their results are not comparable.

We therefore encourage authors, reviewers and editors to enforce a change in the current practice of TWI reporting. To be reproducible and comparable, studies should report the 1) type, version and resolution of the DEM, 2) DEM pre-processing steps, 3) slope algorithm, 4) flow algorithm used to derive the total catchment area and 5) method used to convert the total to specific catchment area.

The selection of the flow algorithm is the most important step affecting TWI performance. The flow algorithm must therefore be specified in all studies using a TWI. In our study, the Freeman FD8 multiple-flow algorithm with a flow dispersion of 1.0 results in the TWI best linked with soil moisture and the moisture-controlled species composition of vascular plants and bryophytes. Based on our results, we therefore recommend total catchment area calculation with the Freeman FD8 flow algorithm and flow dispersion of 1.0, flow width equal to the raster cell size and local slope gradient (Fig. 1).

CRediT authorship contribution statement

Martin Kopecký: Conceptualization, Methodology, Formal analysis, Investigation, Data curation, Writing - original draft, Visualization. **Martin Macek:** Conceptualization, Investigation, Data curation, Writing - review & editing. **Jan Wild:** Conceptualization, Investigation, Writing - review & editing.

Declaration of competing interest

The authors declare that they have no known competing financial interests or personal relationships that could have appeared to influence the work reported in this paper.

Acknowledgements

We thank all colleagues that helped us to collect field data or commented on the manuscript. We also thank both anonymous reviewers for their useful comments.

Funding: This work was supported by the Czech Science Foundation (project 17-13998S) and the Czech Academy of Sciences (project RVO 67985939).

Appendix A. Supplementary data

Supplementary data to this article can be found online at https://doi.org/10.1016/j.scitotenv.2020.143785.

References

Ackerly, D.D., Kling, M.M., Clark, M.L., Papper, P., Oldfather, M.F., Flint, A.L., Flint, L.E., 2020. Topoclimates, refugia, and biotic responses to climate change. Front. Ecol. Environ. 18, 288–297. https://doi.org/10.1002/fee.2204.

Babaeian, E., Sadeghi, M., Jones, S.B., Montzka, C., Vereecken, H., Tuller, M., 2019. Ground, proximal, and satellite remote sensing of soil moisture. Rev. Geophys. 57, 530–616. https://doi.org/10.1029/2018RG000618.

Bauer, J., Rohdenburg, H., Bork, H.R., 1985. Ein Digitales Reliefmodell als Vorraussetzung fuer ein deterministisches Modell der Wasser- und Stoff- Fluesse. In: Bork, H.R., Rohdenburg, H. (Eds.), Parameteraufbereitung fuer deterministische Gebiets-Wassermodelle, Grundlagenarbeiten zu Analyse von Agrar-Oekosystemen. Technische Universität Braunschweig, Braunschweig, DE, pp. 1–15.

Beaudette, D.E., Dahlgren, R.a., O'Geen, A.T., 2013. Terrain-shape indices for modeling soil moisture dynamics. Soil Sci. Soc. Am. J. 77, 1696. https://doi.org/10.2136/sssaj2013.02.0048.

Beven, K.J., Kirkby, M.J., 1979. A physically based, variable contributing area model of basin hydrology. Hydrol. Sci. J. 24, 43–69. https://doi.org/10.1080/02626667909491834.

Böhner, J., Selige, T., 2006. Spatial prediction of soil attributes using terrain analysis and climate regionalisation. SAGA–Analyses and Modelling Applications. Göttinger Geographische Abhandlungen, pp. 13–28.

Breshears, D.D., Myers, O.B., Barnes, F.J., 2009. Horizontal heterogeneity in the frequency of plant-available water with woodland intercanopy - canopy vegetation patch type rivals that occuring vertically by soil depth. Ecohydrology 2, 503–519. https://doi.org/10.1002/eco.75.

Buchanan, B.P., Fleming, M., Schneider, R.L., Richards, B.K., Archibald, J., Qiu, Z., Walter, M.T., 2014. Evaluating topographic wetness indices across central New York agricultural landscapes. Hydrol. Earth Syst. Sci. 18, 3279–3299. https://doi.org/10.5194/hess-18-3279-2014.

Buytaert, W., Reusser, D., Krause, S., Renaud, J.-P., 2008. Why can't we do better than Topmodel? Hydrol. Process. 22, 4175–4179. https://doi.org/10.1002/hyp.7125.

Chirico, G.B., Western, A.W., Grayson, R.B., Blöschl, G., 2005. On the definition of the flow width for calculating specific catchment area patterns from gridded elevation data. Hydrol. Process. 19, 2539–2556. https://doi.org/10.1002/hyp.5730.

Conrad, O., Bechtel, B., Bock, M., Dietrich, H., Fischer, E., Gerlitz, L., Wehberg, J., Wichmann, V., Böhner, J., 2015. System for Automated Geoscientific Analyses (SAGA) v. 2.1.4. Geosci. Model Dev. 8, 1991–2007. https://doi.org/10.5194/gmd-8-1991-2015.

Costa-Cabral, M., Burges, S., 1994. Digital elevation model networks (DEMON): a model of flow over hillslopes for computation of contributing and dispersal areas. Water Resour. Res. 30, 1681–1692.

Erskine, R.H., Green, T.R., Ramirez, J.a., MacDonald, L.H., 2006. Comparison of grid-based algorithms for computing upslope contributing area. Water Resour. Res. 42, 1–9. https://doi.org/10.1029/2005WR004648.

Fairfield, J., Leymarie, P., 1991. Drainage networks from grid digital elevation models. Water Resour. Res. 27, 709–717. https://doi.org/10.1029/90WR02658.

Fan, Y., Clark, M., Lawrence, D.M., Swenson, S., Band, L.E., Brantley, S.L., Brooks, P.D., Dietrich, W.E., Flores, A., Grant, G., Kirchner, J.W., Mackay, D.S., McDonnell, J.J., Milly, P.C.D., Sullivan, P.L., Tague, C., Ajami, H., Chaney, N., Hartmann, A., Hazenberg, P., McNamara, J., Pelletier, J., Perket, J., Rouholahnejad-Freund, E., Wagener, T., Zeng, X., Beighley, E., Buzan, J., Huang, M., Livneh, B., Mohanty, B.P., Nijssen, B., Safeeq, M., Shen, C., Verseveld, W., Volk, J., Yamazaki, D., 2019. Hillslope hydrology in global change research and earth system modeling. Water Resour. Res. 55, 1737–1772. https://doi.org/10.1029/2018WR023903.

Freeman, T., 1991. Calculating catchment area with divergent flow based on a regular grid. Comput. Geosci. 17, 413–422. https://doi.org/10.1016/0098-3004(91)90048-I.

Goebes, P., Schmidt, K., Seitz, S., Both, S., Bruelheide, H., Erfmeier, A., Scholten, T., Kühn, P., 2019. The strength of soil-plant interactions under forest is related to a Critical Soil Depth. Sci. Rep. 9, 8635. https://doi.org/10.1038/s41598-019-45156-5.

Greiser, C., Meineri, E., Luoto, M., Ehrlén, J., Hylander, K., 2018. Monthly microclimate models in a managed boreal forest landscape. Agric. For. Meteorol. 250–251, 147–158. https://doi.org/10.1016/j.agrformet.2017.12.252.

Gruber, S., Peckham, S., 2009. Land-surface parameters and objects in hydrology. Dev. Soil Sci., 171–194 https://doi.org/10.1016/S0166-2481(08)00007-X.

Haralick, R.M., 1983. Ridges and valleys on digital images. Comput. Vision, Graph. Image Process. 22, 28–38. https://doi.org/10.1016/0734-189X(83)90094-4.

Heerdegen, R.G., Beran, M.A., 1982. Quantifying source areas through land surface curvature and shape. J. Hydrol. 57, 359–373. https://doi.org/10.1016/0022-1694(82)90155-X.

Hjerdt, K.N., McDonnell, J.J., Seibert, J., Rodhe, A., 2004. A new topographic index to quantify downslope controls on local drainage. Water Resour. Res. 40, 1–6. https://doi.org/10.1029/2004WR003130.

Holmgren, P., 1994. Multiple flow direction algorithms for runoff modelling in grid based elevation models: an empirical evaluation. Hydrol. Process. 8, 327–334. https://doi.org/10.1002/hyp.3360080405.

Horn, B.K.P., 1981. Hill shading and the reflectance map. Proc. IEEE 69, 14–47. https://doi.org/10.1109/PROC.1981.11918.

Huntley, B., Allen, J.R.M., Bennie, J., Collingham, Y.C., Miller, P.A., Suggitt, A.J., 2017. Climatic disequilibrium threatens conservation priority forests. Conserv. Lett. (1), 1–9 https://doi.org/10.1111/conl.12349.

Jones, K., 1998. A comparison of algorithms used to compute hill slope as a property of the DEM. Comput. Geosci. 24, 315–323. https://doi.org/10.1016/S0098-3004(98)00032-6.

Kemppinen, J., Niittynen, P., Riihimäki, H., Luoto, M., 2018. Modelling soil moisture in a high-latitude landscape using LiDAR and soil data. Earth Surf. Process. Landforms 43, 1019–1031. https://doi.org/10.1002/esp.4301.

Kemppinen, J., Niittynen, P., Aalto, J., le Roux, P.C., Luoto, M., 2019. Water as a resource, stress and disturbance shaping tundra vegetation. Oikos 128, 811–822. https://doi.org/10.1111/oik.05764.

Kopecký, M., Čížková, Š., 2010. Using Topographic Wetness Index in vegetation ecology: does the algorithm matter? Appl. Veg. Sci. 13, 450–459. https://doi.org/10.1111/j.1654-109X.2010.01083.x.

Lanni, C., McDonnell, J.J., Rigon, R., 2011. On the relative role of upslope and downslope topography for describing water flow path and storage dynamics: a theoretical analysis. Hydrol. Process. 25, 3909–3923. https://doi.org/10.1002/hyp.8263.

le Roux, P.C., Aalto, J., Luoto, M., 2013. Soil moisture's underestimated role in climate change impact modelling in low-energy systems. Glob. Chang. Biol. 19, 2965–2975. https://doi.org/10.1111/gcb.12286.

Lea, N.L., 1992. An aspect driven kinematic routing algorithm. In: Parsons, A.J., Abrahams, A.D. (Eds.), Overland Flow: Hydraulics and Erosion Mechanics. Chapman & Hall, New York, NY, USA, pp. 393–407.

Legendre, P., Lengendre, L., 2012. Numerical ecology. Elsevier.

Lookingbill, T., Urban, D., 2004. An empirical approach towards improved spatial estimates of soil moisture for vegetation analysis. Landsc. Ecol. 19, 417–433. https://doi.org/10.1023/B:LAND.0000030451.29571.8b.

Macek, M., Kopecký, M., Wild, J., 2019. Maximum air temperature controlled by landscape topography affects plant species composition in temperate forests. Landsc. Ecol. 34, 2541–2556. https://doi.org/10.1007/s10980-019-00903-x.

Maclean, I.M.D., 2020. Predicting future climate at high spatial and temporal resolution. Glob. Chang. Biol. 26, 1003–1011. https://doi.org/10.1111/gcb.14876.

Martin, J., Looker, N., Hoylman, Z., Jencso, K., Hu, J., 2017. Hydrometeorology organizes intra-annual patterns of tree growth across time, space and species in a montane watershed. New Phytol. 215, 1387–1398. https://doi.org/10.1111/nph.14668.

Mattivi, P., Franci, F., Lambertini, A., Bitelli, G., 2019. TWI computation: a comparison of different open source GISs. Open Geospatial Data, Softw. Stand. 4, 6. https://doi.org/10.1186/s40965-019-0066-y.

McArdle, B.H., Anderson, M.J., 2001. Fitting multivariate models to community data: a comment on distance-based redundancy analysis. Ecology 82, 290–297. https://doi.org/10.1890/0012-9658(2001)082[0290:FMMTCD]2.0.CO;2.

McGregor, I.R., Helcoski, R., Kunert, N., Tepley, A.J., Gonzalez-Akre, E.B., Herrmann, V., Zailaa, J., Stovall, A.E., Bourg, N.A., McShea, W.J., Pederson, N., Sack, L., Anderson-Teixeira, K.J., 2020. Tree height and leaf drought tolerance traits shape growth responses across droughts in a temperate broadleaf forest. New Phytol. https://doi.org/10.1111/nph.16996.

McLaughlin, B.C., Blakey, R., Weitz, A.P., Feng, X., Brown, B.J., Ackerly, D.D., Dawson, T.E., Thompson, S.E., 2020. Weather underground: subsurface hydrologic processes mediate tree vulnerability to extreme climatic drought. Glob. Chang. Biol. 26, 3091–3107. https://doi.org/10.1111/gcb.15026.

Metcalfe, P., Beven, K., Freer, J., 2015. Dynamic TOPMODEL: a new implementation in R and its sensitivity to time and space steps. Environ. Model. Softw. 72, 155–172. https://doi.org/10.1016/j.envsoft.2015.06.010.

Metzen, D., Sheridan, G.J., Benyon, R.G., Bolstad, P.V., Griebel, A., Lane, P.N.J., 2019. Spatiotemporal transpiration patterns reflect vegetation structure in complex upland terrain. Sci. Total Environ. 694, 133551. https://doi.org/10.1016/j.scitotenv.2019.07.357.

Moeslund, J.E., Zlinszky, A., Ejrnæs, R., Brunbjerg, A.K., Bøcher, P.K., Svenning, J.C., Normand, S., 2019. Light detection and ranging explains diversity of plants, fungi, lichens, and bryophytes across multiple habitats and large geographic extent. Ecol. Appl. 29, 1–17. https://doi.org/10.1002/eap.1907.

Moore, I.D., Grayson, R.B., Ladson, A.R., 1991. Digital terrain modelling: a review of hydrological, geomorphological, and biological applications. Hydrol. Process. 5, 3–30. https://doi.org/10.1002/hyp.3360050103.

Muscarella, R., Kolyaie, S., Morton, D.C., Zimmerman, J.K., Uriarte, M., 2020. Effects of topography on tropical forest structure depend on climate context. J. Ecol. 108, 145–159. https://doi.org/10.1111/1365-2745.13261.

O'Callaghan, J.F., Mark, D.M., 1984. The extraction of drainage networks from digital elevation data. Comput. Vision, Graph. Image Process 47, 323–344.
Oksanen, J., Blanchet, F.G., Friendly, M., Kindt, R., Legendre, P., McGlinn, D., Minchin, P.R., O'Hara, R.B., Simpson, G.L., Solymos, P., Stevens, M.H.H., Szoecs, E., Wagner, H., 2019. Vegan: Community Ecology Package. R package version 2.5-6 https://CRAN.R-project.org/package=vegan.
Oroza, C.A., Bales, R.C., Stacy, E.M., Zheng, Z., Glaser, S.D., 2018. Long-term variability of soil moisture in the southern sierra: measurement and prediction. Vadose Zo. J. 17, 170178. https://doi.org/10.2136/vzj2017.10.0178.
Pan, F., Peters-Lidard, C.D., Sale, M.J., King, A.W., 2004. A comparison of geographical information systems-based algorithms for computing the TOPMODEL topographic index. Water Resour. Res. 40, 1–11. https://doi.org/10.1029/2004WR003069.
Piedallu, C., Gégout, J., Perez, V., Lebourgeois, F., 2013. Soil water balance performs better than climatic water variables in tree species distribution modelling. Glob. Ecol. Biogeogr. 22, 470–482. https://doi.org/10.1111/geb.12012.
Piedallu, C., Chéret, V., Denux, J.P., Perez, V., Azcona, J.S., Seynave, I., Gégout, J.C., 2019. Soil and climate differently impact NDVI patterns according to the season and the stand type. Sci. Total Environ. 651, 2874–2885. https://doi.org/10.1016/j.scitotenv.2018.10.052.
Qin, C., Zhu, A.-X.-X., Pei, T., Li, B., Zhou, C., Yang, L., 2007. An adaptive approach to selecting a flow-partition exponent for a multiple-flow-direction algorithm. Int. J. Geogr. Inf. Sci. 21, 443–458. https://doi.org/10.1080/13658810601073240.
Quinn, P., Beven, K., Chevallier, P., Planchon, O., 1991. The prediction of hillslope flow paths for distributed hydrological modelling using digital terrain models. Hydrol. Process. 5, 59–79. https://doi.org/10.1002/hyp.3360050106.
R Core Team, 2020. R: A language and environment for statistical computing. R Foundation for Statistical Computing, Vienna, Austria https://www.R-project.org/.
Raduła, M.W., Szymura, T.H., Szymura, M., 2018. Topographic Wetness Index explains soil moisture better than bioindication with Ellenberg's indicator values. Ecol. Indic. 85, 172–179. https://doi.org/10.1016/j.ecolind.2017.10.011.
Robinson, D.A., Campbell, C.S., Hopmans, J.W., Hornbuckle, B.K., Jones, S.B., Knight, R., Ogden, F., Selker, J., Wendroth, O., 2008. Soil moisture measurement for ecological and hydrological watershed-scale observatories: a review. Vadose Zo. J. 7, 358. https://doi.org/10.2136/vzj2007.0143.
Schmitt, S., Hérault, B., Ducouret, É., Baranger, A., Tysklind, N., Heuertz, M., Marcon, É., Cazal, S.O., Derroire, G., 2020. Topography consistently drives intra- and interspecific leaf trait variation within tree species complexes in a Neotropical forest. Oikos 129, 1521–1530. https://doi.org/10.1111/oik.07488.
Schwantes, A.M., Parolari, A.J., Swenson, J.J., Johnson, D.M., Domec, J.C., Jackson, R.B., Pelak, N., Porporato, A., 2018. Accounting for landscape heterogeneity improves spatial predictions of tree vulnerability to drought. New Phytol. 220, 132–146. https://doi.org/10.1111/nph.15274.
Seibert, J., McGlynn, B.L., 2007. A new triangular multiple flow direction algorithm for computing upslope areas from gridded digital elevation models. Water Resour. Res. 43, 1–8. https://doi.org/10.1029/2006WR005128.
Seibert, J., Stendahl, J., Sørensen, R., 2007. Topographical influences on soil properties in boreal forests. Geoderma 141, 139–148. https://doi.org/10.1016/j.geoderma.2007.05.013.
Sørensen, R., Seibert, J., 2007. Effects of DEM resolution on the calculation of topographical indices: TWI and its components. J. Hydrol. 347, 79–89. https://doi.org/10.1016/j.jhydrol.2007.09.001.
Sørensen, R., Zinko, U., Seibert, J., 2006. On the calculation of the topographic wetness index: evaluation of different methods based on field observations. Hydrol. Earth Syst. Sci. 10, 101–112. https://doi.org/10.5194/hess-10-101-2006.
Stichbury, G., Brabyn, L., Green, T.G.A., Cary, C., 2011. Spatial modelling of wetness for the Antarctic dry valleys. Polar Res. 30, 6330. https://doi.org/10.3402/polar.v30i0.6330.
Tang, J., Pilesjö, P., Persson, A., 2013. Estimating slope from raster data - a test of eight algorithms at different resolutions in flat and steep terrain. Geod. Cartogr. 39, 41–52. https://doi.org/10.3846/20296991.2013.806702.
Tang, J., Miller, P.A., Crill, P.M., Olin, S., Pilesjö, P., 2015. Investigating the influence of two different flow routing algorithms on soil-water-vegetation interactions using the dynamic ecosystem model LPJ-GUESS. Ecohydrology 8, 570–583. https://doi.org/10.1002/eco.1526.
Tarboton, D.G., 1997. A new method for the determination of flow directions and upslope areas in grid digital elevation models. Water Resour. Res. 33, 309. https://doi.org/10.1029/96WR03137.
Travis, M.R., Elsner, G.H., Iverson, W.D., Johnson, C.G., 1975. VIEWIT: Computation of Seen Areas, Slope, and Aspect for Land-Use Planning. USDA F.S. Gen. Tech. Rep, Berkeley, California, USA.
Vanwalleghem, T., Meentemeyer, R.K., 2009. Predicting forest microclimate in heterogeneous landscapes. Ecosystems 12, 1158–1172. https://doi.org/10.1007/s10021-009-9281-1.
Wang, L., Liu, H., 2006. An efficient method for identifying and filling surface depressions in digital elevation models for hydrologic analysis and modelling. Int. J. Geogr. Inf. Sci. 20, 193–213. https://doi.org/10.1080/13658810500433453.
Warren, S.D., Hohmann, M.G., Auerswald, K., Mitasova, H., 2004. An evaluation of methods to determine slope using digital elevation data. Catena 58, 215–233. https://doi.org/10.1016/j.catena.2004.05.001.
Western, A.W.A., Grayson, R.R.B., Willgoose, G.R., Mcmahon, T.A., 1999. Observed spatial organization of soil moisture and its relation to terrain indices. Water Resour. Res. 35, 797–810. https://doi.org/10.1029/1998WR900065.
Wietrzyk-Pełka, P., Rola, K., Szymański, W., Węgrzyn, M.H., 2020. Organic carbon accumulation in the glacier forelands with regard to variability of environmental conditions in different ecogenesis stages of high Arctic ecosystems. Sci. Total Environ. 717, 135151. https://doi.org/10.1016/j.scitotenv.2019.135151.
Wild, J., Kopecký, M., Macek, M., Šanda, M., Jankovec, J., Haase, T., 2019. Climate at ecologically relevant scales: a new temperature and soil moisture logger for long-term microclimate measurement. Agric. For. Meteorol. 268, 40–47. https://doi.org/10.1016/j.agrformet.2018.12.018.
Wilson, J.P., 2018. Calculating land surface parameters. Environmental Applications of Digital Terrain Modeling, pp. 53–149 https://doi.org/10.1002/9781118938188.ch3.
Wilson, J.P., Lam, C.S., Deng, Y., 2007. Comparison of the performance of flow-routing algorithms used in GIS-based hydrologic analysis. Hydrol. Process. 1044, 1026–1044. https://doi.org/10.1002/hyp.
Wolock, D., McCabe, G., 1995. Comparison of single and multiple flow direction algorithms for computing topographic parameters in TOPMODEL. Water Resour. Res. 31, 1315–1324.
Yeakley, J.A., Swank, W.T., Swift, L.W., Hornberger, G.M., Shugart, H.H., 1998. Soil moisture gradients and controls on a southern Appalachian hillslope from drought through recharge. Hydrol. Earth Syst. Sci. 2, 41–49. https://doi.org/10.5194/hess-2-41-1998.
Zellweger, F., Braunisch, V., Morsdorf, F., Baltensweiler, A., Abegg, M., Roth, T., Bugmann, H., Bollmann, K., 2015. Disentangling the effects of climate, topography, soil and vegetation on stand-scale species richness in temperate forests. For. Ecol. Manag. 349, 36–44. https://doi.org/10.1016/j.foreco.2015.04.008.
Zevenbergen, L.W., Thorne, C.R., 1987. Quantitative analysis of land surface topography. Earth Surf. Process. Landforms 12, 47–56. https://doi.org/10.1002/esp.3290120107.
Zhou, Q., Liu, X., 2002. Error assessment of grid-based flow routing algorithms used in hydrological models. Int. J. Geogr. Inf. Sci. 16, 819–842. https://doi.org/10.1080/13658810210149425.
Zinko, U., Dynesius, M., Nilsson, C., Seibert, J., 2006. The role of soil pH in linking groundwater flow and plant species density in boreal forest landscapes. Ecography 29, 515–524. https://doi.org/10.1111/j.0906-7590.2006.04581.x.